Electronic Supplementary Material (ESI) for Physical Chemistry Chemical Physics.

Supporting Information

Janus CrSSe Monolayer with an Interesting Ferromagnetism

Fanjunjie Han[a], Xu Yan[b], Aitor Bergara[c,d,e,*], Wenjing Li[a], Hong Yu[a], and Guochun Yang[a,b,*]

[a]*Centre for Advanced Optoelectronic Functional Materials Research and Key Laboratory for UV Light-Emitting Materials and Technology of Ministry of Education, Northeast Normal University, Changchun 130024, China*

[b]*State Key Laboratory of Metastable Materials Science & Technology and Key Laboratory for Microstructural Material Physics of Hebei Province, School of Science, Yanshan University, Qinhuangdao 066004, China*

[c]*Departmento de Física and EHU Quantum Center, Universidad del País Vasco, UPV/EHU, 48080 Bilbao, Spain*

[d]*Donostia International Physics Center (DIPC), 20018 Donostia, Spain*

[e]*Centro de Física de Materiales CFM, Centro Mixto CSIC-UPV/EHU, 20018 Donostia, Spain*

Index **page**

Computational Details

The particle swarm optimization (PSO) method within the evolutionary algorithm as implemented in the Crystal structure AnaLYsis by Particle Swarm Optimization (CALYPSO) code[1,2] was applied to find new structures of CrSSe monolayers. Unit cells containing 1, and 2 formula units (f.u.) were considered. In the first step, random structures with certain symmetry are constructed in which atomic coordinates are generated by the crystallographic symmetry operations. Local optimizations using the VASP code[3] were done with the conjugate gradients method and stopped when Gibbs free energy changes became smaller than 1×10^{-5} eV per cell. After processing the first-generation structures, 60% of them with lowest Gibbs free energies are selected to construct the next generation structures by PSO. 40% of the structures in the new generation are randomly generated. A structure fingerprinting technique of bond characterization matrix is applied to the generated structures, so that identical structures are strictly forbidden. These procedures significantly enhance the diversity of the structures, which is crucial for structural global search efficiency. In most cases, structural searching simulations for each calculation were stopped after generating 1000~ 1200 structures (e.g., about 20 ~ 30 generations).

The local structural relaxations and electronic property calculations were performed in the framework of the density functional theory (DFT)[4] within the generalized gradient approximation (GGA)[5] as implemented in the VASP code. The projector augmented wave (PAW) method is used to treat the ion-electron interaction, in which the valence electrons of each atom are Cr: $3d^5 4s^1$, S: $3s^2 3p^4$, Se: $4s^2 4p^4$.

We calculated the cohesive energy of the Janus CrSSe monolayer by using the following expression:

$$E_{coh} = (E_{Cr} + E_S + E_{Se} - E_{CrSSe})/3,$$

where E_{Cr}, E_{S}, E_{Se} and E_{CrSSe} are the total energies of a single Cr atom, S atom, Se atom and the Janus CrSSe monolayer, respectively.

The Young's modulus $Y(\theta)$ and Poisson's ratio $v(\theta)$ along any direction θ (θ is the angle with respect to the positive x-direction) are defined as

$$Y(\theta) = \frac{C_{11}C_{22} - C_{12}^2}{C_{11}s^4 + C_{22}c^4 + (\frac{C_{11}C_{22} - C_{12}^2}{C_{66}} - 2C_{12})c^2s^2}$$

$$\nu(\theta) = \frac{C_{12}(c^4 + s^4) - (C_{11} + C_{22} - \frac{C_{11}C_{22} - C_{12}^2}{C_{66}})c^2s^2}{C_{11}s^4 + C_{22}c^4 + (\frac{C_{11}C_{22} - C_{12}^2}{C_{66}} - 2C_{12})c^2s^2}$$

were c = $\cos\theta$ and s = $\sin\theta$.

Based on the Heisenberg model, the different magnetic configurations for the Janus CrSSe monolayers are given by the following expressions:

$E_{FM} = E_0 - 4J_1\vec{S}^2 - 4J_2\vec{S}^2$

$E_{AFM1} = E_0 - 4J_1\vec{S}^2 + 4J_2\vec{S}^2$

$E_{AFM2} = E_0 + 4J_1\vec{S}^2 + 4J_2\vec{S}^2$

were E_0 is the energy without magnetic coupling, and *S* is set to 1.5. Hence, we can estimate the magnetic coupling parameters J_1 and J_2 by solving these three equations.

The Curie temperature was calculated by the Monte Carlo method with the Metropolis algorithm based on the Heisenberg model. All of them were implemented in MCSOLVER.[6]

Supporting Figures and Tables

Table S1. Structural parameters of the predicted Janus CrSSe monolayer: space group (SG), lattice constants *a* and *b*, layer thickness *h*, bond lengths of Cr-S d_1 and Cr-Se d_2, and bond angles of Cr-S-Cr θ_1 and Cr-Se-Cr θ_2.

	SG	*a* (Å)	*b* (Å)	*h* (Å)	d_1 (Å)	d_2 (Å)	θ_1 (°)	θ_2 (°)
CrSSe	*Pmm*2	3.58	3.65	2.66	2.17	2.32	111.0	104.0

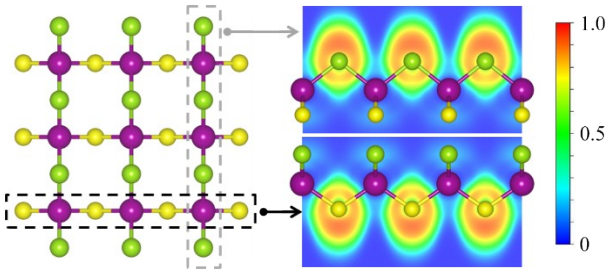

Fig. S1. ELF maps of different interfaces in the Janus CrSSe monolayer.

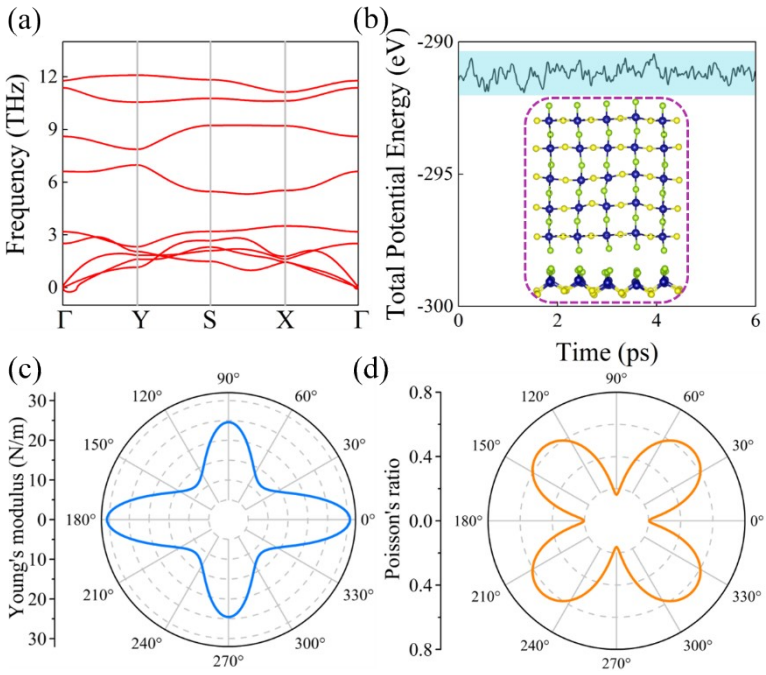

Fig. S2. (a) Phonon dispersion curves, (b) total energies and the snapshots of the final frame, and (c, d) orientation-dependent in plane Young's modulus $Y(\theta)$ and Poisson's ratio $\nu(\theta)$ of the Janus CrSSe monolayer.

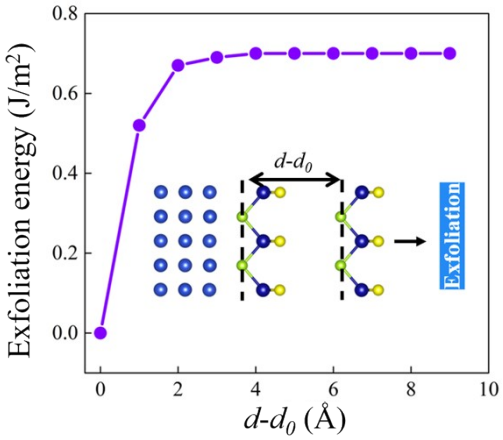

Fig. S3. Calculated exfoliation energy of the Janus CrSSe monolayer deposited on the Cu (001) surface.

To find out whether the Janus CrSSe monolayer can be synthesized experimentally on a substrate, we have examined its stability on several substrates, such as Cu (001), Ag (001), Au (001) and graphene, which are widely used for surface growth in experiments. Finally, our calculations show that the Janus CrSSe monolayer remains stable on the Cu (001) substrate. The mismatch between the Janus CrSSe (a = 7.165 Å) and the Cu (001) (a = 7.213 Å) is 0.7%, which is suitable for the formation of the heterostructure made by 2D Janus CrSSe and Cu (001) surface. Subsequently, to explore the possibility of fabricating the Janus CrSSe monolayer deposited on the Cu (001) surface, we have simulated the exfoliation process and predicted exfoliation energy with respect to separation. The calculated exfoliation energy of the Janus CrSSe monolayer is 0.7 J/m^2, which is comparable to the δ-InP_3 (0.827 J/m^2)[7] and SnP_3 (0.71 J/m^2),[8] indicating the Janus CrSSe monolayer could be prepared experimentally from Cu (001) surface from using similar approaches as graphene by mechanical cleavage or liquid phase exfoliation.

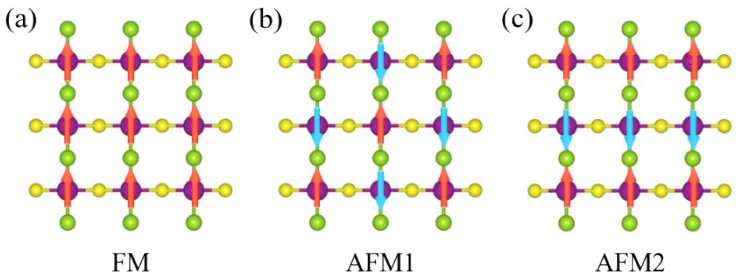

Fig. S4. Considered different magnetic configurations: FM, AFM1, and AFM2 of the Janus CrSSe monolayer in a 2×2×1 supercell. Red and blue arrows denote spin-up and spin-down states, respectively.

Table S2. Total energies of the Janus CrSSe monolayer under different magnetic configurations. (Considering the SOC selects the direction of the spin state along out-of-plane.)

		FM	AFM1	AFM2
CrSSe	GGA+U	**-61.335014**	-59.533385	-60.667903
	GGA+U+SOC	**-61.454120**	-59.651125	-60.788104

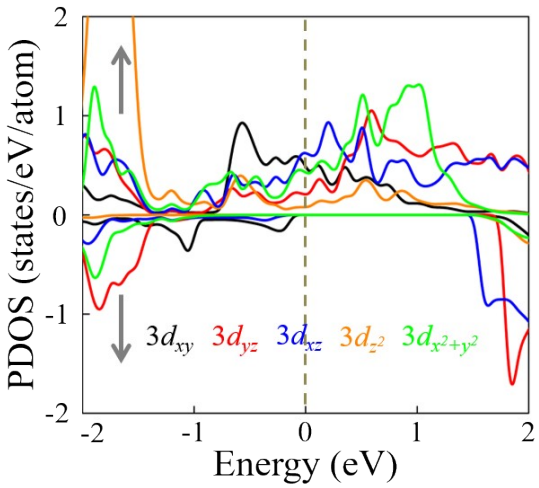

Fig. S5. PDOS onto five partial 3*d* orbitals of Cr atoms of the FM Janus CrSSe monolayer.

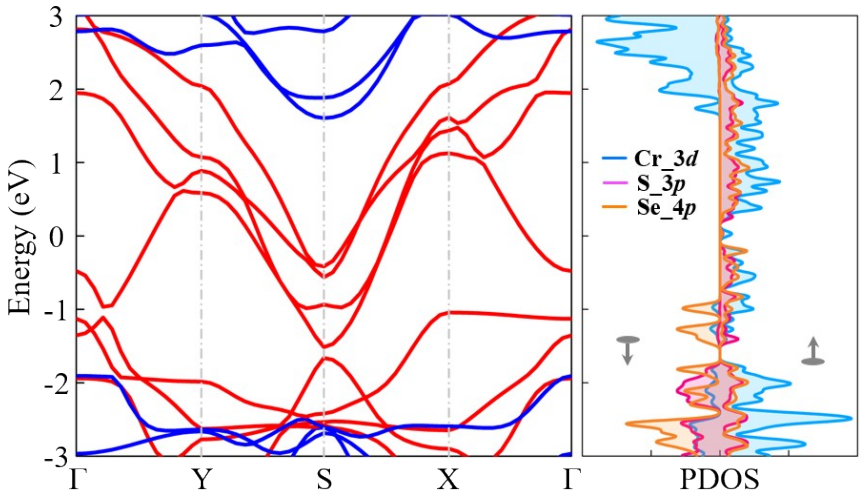

Fig. S6. Band structures and spin-resolved PDOS of the FM Janus CrSSe monolayer at the hybrid HSE06 level. The red and blue lines indicate the spin-up and spin-down states, respectively.

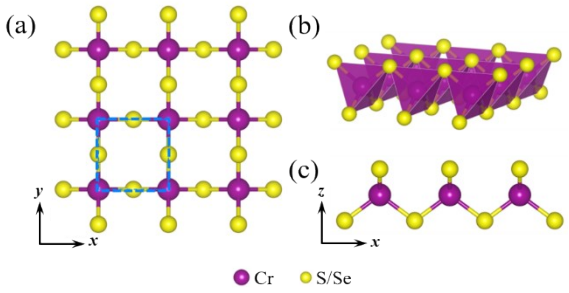

Fig. S7. Geometry of structures of CrS_2 and $CrSe_2$ monolayers.

Table S3. Structural parameters of the CrS_2 and $CrSe_2$ monolayers: space group (SG), lattice constants a and b, layer thickness h, bond lengths of Cr-S d_1 and Cr-Se d_2, bond angles of Cr-S-Cr θ_1, Cr-Se-Cr θ_2 and cohesive energy E_{coh}.

Systems	SG	a (Å)	b (Å)	h (Å)	d_1 (Å)	d_2 (Å)	θ_1 (°)	θ_2 (°)	E_{coh} (eV)
CrS_2	*P*-4*m*2	3.53	3.53	2.56	2.18	/	108.2	/	3.92
$CrSe_2$	*P*-4*m*2	3.70	3.70	2.77	/	2.31	/	106.3	3.46

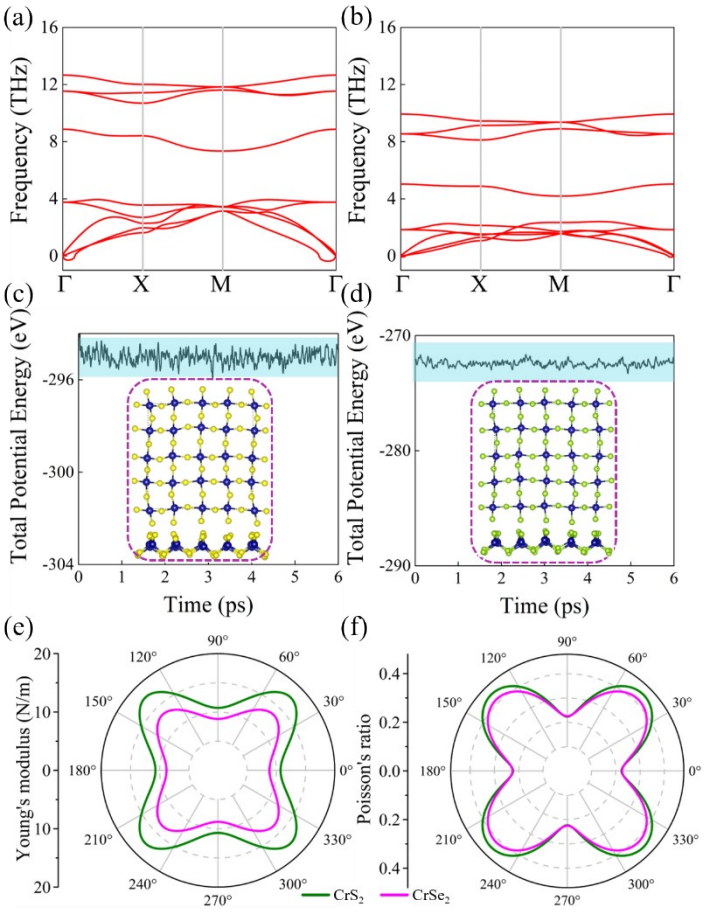

Fig. S8. Calculated structural stabilities of (a, c) CrS_2 and (b, d) $CrSe_2$ monolayers. (e, f) $Y(\theta)$ and $\nu(\theta)$.

Table S4. Elastic constants (C_{11}, C_{12}, C_{66}, in N/m), Young's modulus and Poisson's ratio of the CrS_2

and $CrSe_2$ monolayers.

	C_{11} (N/m)	C_{12} (N/m)	C_{66} (N/m)	Y_{max}	Y_{min}	ν_{max}	ν_{min}
CrS_2	45.39	10.14	10.71	43.12	30.91	0.44	0.22
$CrSe_2$	34.74	7.83	8.82	32.97	24.93	0.41	0.23

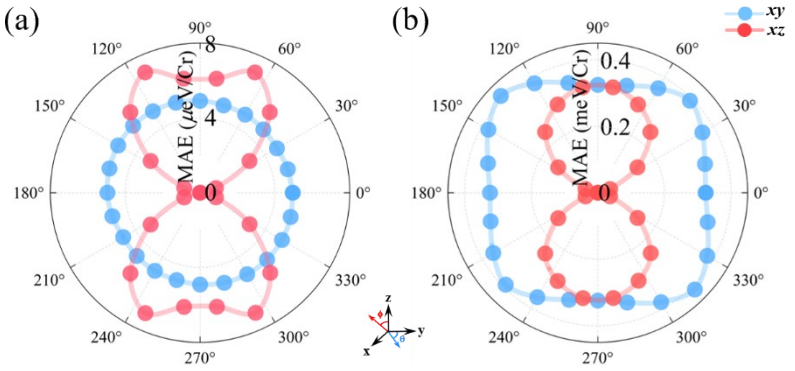

Fig. S9. Angular dependence of the magnetic anisotropy energy (MAE) of the (a) CrS_2 and (b) $CrSe_2$ monolayers.

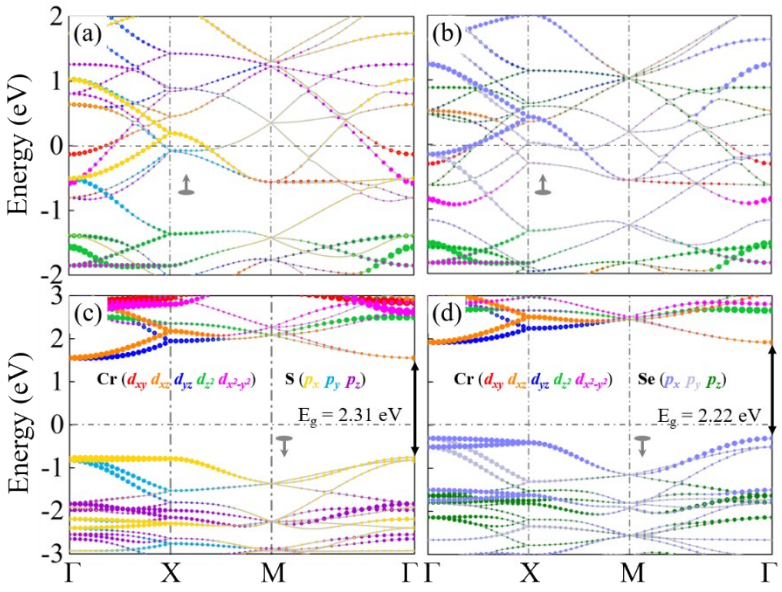

Fig. S10. Projected band structures with spin-up and spin-down states for (a, c) CrS_2, and (b, d) $CrSe_2$ monolayers. The Fermi level is set to 0 eV. The 2.31 and 2.22 eV direct band-gap in spin-down channel are illustrated.

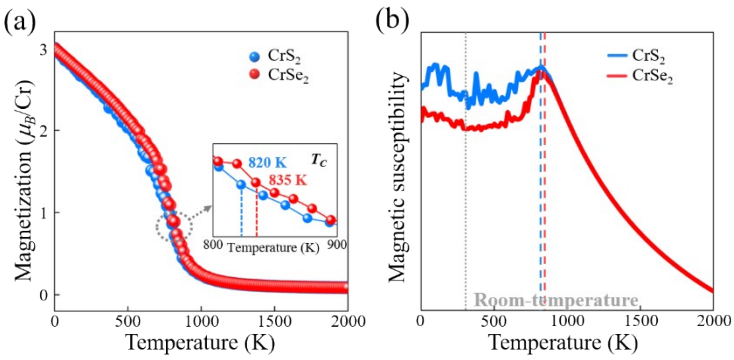

Fig. S11. (a) Calculated average magnetic moment of Cr atoms and (b) magnetic susceptibility with respect to temperature of the CrS_2 and $CrSe_2$ monolayers based on the Heisenberg model from MC simulations.

Table S5. Data related to the CrS_2 and $CrSe_2$ monolayers, including local magnetic moment on Cr, S and Se atoms, magnetic exchange constants J_1 and J_2, evaluated Curie temperatures (T_C), maximum magnetic anisotropy energy (MAE_{max}) and the band-gaps (E_g).

systems	M_{Cr} (μ_B)	M_S (μ_B)	M_{Se} (μ_B)	J_1 (meV)	J_2 (meV)	T_C (K)	MAE_{max} (μeV/Cr)	E_g (eV)
CrS_2	2.93	-0.36	/	49.92	/	820	7.07	0/2.31
$CrSe_2$	3.24	/	-0.46	50.47	/	835	411.65	0/2.22

Table S6. Total energies of the CrS_2 and $CrSe_2$ monolayers under different magnetic configurations. (Considering the SOC selects the direction of spin state along the out-of-plane.)

		FM	AFM1	AFM2
CrS_2	GGA+U	**-64.282332**	-62.493469	-63.293510
	GGA+U+SOC	**-64.310923**	-62.513796	-63.317936
$CrSe_2$	GGA+U	**-58.380705**	-56.542859	-57.526540
	GGA+U+SOC	**-58.587884**	-56.771095	-57.739471

Table S7. Structural information of the predicted 2D CrSSe, CrS_2, and $CrSe_2$ monolayers.

	Space Group	Lattice Parameters (Å, °)	Wyckoff Positions (fractional) Atoms	*x*	*y*	*z*
CrSSe	*Pmm*2	*a*= 3.5872	Cr(1a)	0.00000	0.00000	0.49820
		b= 3.6538	Se(1b)	0.00000	0.50000	0.53705
		α=*β*=*γ*= 90.00	S (1c)	0.50000	0.00000	0.46475
CrS_2	*P*-4*m*2	*a*=*b*= 3.5293	Cr(1d)	0.00000	0.00000	0.50000
		α=*β*=*γ*= 90.00	S(2g)	0.00000	0.50000	0.53546
$CrSe_2$	*P*-4*m*2	*a*=*b*= 3.7006	Cr(1d)	0.00000	0.00000	0.50000
		α=*β*=*γ*= 90.00	Se(2g)	0.00000	0.50000	0.53724

References

1 Y. Wang, J. Lv, L. Zhu and Y. Ma, *Comput. Phys. Commun.*, 2012, **183**, 2063–2070.

2 Y. Wang, J. Lv, L. Zhu and Y. Ma, *Phys. Rev. B*, 2010, **82**, 94116.

3 G. Kresse and J. Furthmu, *Phys. Rev. B.*, 1996, **54**, 11169.

4 W. Kohn and L. J. Sham, *Phys. Rev.*, 1965, **140**, A1133–A1138.

5 J. P. Perdew, K. Burke and M. Ernzerhof, *Phys. Rev. Lett.*, 1996, **77**, 3865.

6 L. Liu, X. Ren, J. Xie, B. Cheng, W. Liu, T. An, H. Qin and J. Hu, *Appl. Surf. Sci.*, 2019, **480**, 300–307.

7 W. Yi, X. Chen, Z. Wang, Y. Ding, B. Yang and X. Liu, *J. Mater. Chem. C*, 2019, **7**, 7352–7359.

8 B. Ghosh, S. Puri, A. Agarwal and S. Bhowmick, *J. Phys. Chem. C*, 2018, **122**, 18185–18191.